Geochemical Journal, Vol. 50, pp. 591 to 603, 2016 doi:10.2343/geochemj.2.0435

Geological factors responsible for REY-rich mud in the western North Pacific Ocean: Implications from mineralogy and grain size distributions

Junichiro Ohta,[1] Kazutaka Yasukawa,[2,3] Shiki Machida,[4] Koichiro Fujinaga,[3] Kentaro Nakamura,[2] Yutaro Takaya,[5] Koichi Iijima,[4] Katsuhiko Suzuki[4] and Yasuhiro Kato[2,3,4,6]*

[1]Department of Solid Earth Geochemistry, Japan Agency for Marine-Earth Science and Technology (JAMSTEC), 2-15 Natsushima-cho, Yokosuka, Kanagawa 237-0061, Japan
[2]Department of Systems Innovation, School of Engineering, The University of Tokyo, 7-3-1 Hongo, Bunkyo-ku, Tokyo 113-8656, Japan
[3]Ocean Resources Research Center for Next Generation, Chiba Institute of Technology, 2-17-1 Tsudanuma, Narashino, Chiba 275-0016, Japan
[4]Research and Development Center for Submarine Resources, Japan Agency for Marine-Earth Science and Technology (JAMSTEC), 2-15 Natsushima-cho, Yokosuka, Kanagawa 237-0061, Japan
[5]Department of Resources and Environmental Engineering, School of Creative Science and Engineering, Waseda University, 3-4-1 Okubo, Shinjyuku-ku, Tokyo 169-8555, Japan
[6]Frontier Research Center for Energy and Resources, School of Engineering, The University of Tokyo, 7-3-1 Hongo, Bunkyo-ku, Tokyo 113-8656, Japan

(*Received March 26, 2015; Accepted July 15, 2016*)

Seven piston cores were collected from the seafloor ~250 km south of Minamitorishima Island in the western North Pacific Ocean during the cruise KR13-02 of *R/V Kairei*; in some portions of cores PC04 and PC05, the total contents of rare-earth elements and yttrium (∑REY) exceeded 4,000 ppm. Microscopic observations showed that the highly REY-enriched layers (∑REY > ~2,000 ppm) contained significant amounts of calcium phosphate and phillipsite. We conducted microscopic observations and grain size distribution analyses of bulk sediments and distinctive components (calcium phosphate and phillipsite) from cores PC04 and PC05 to elucidate the mechanism of the anomalous REY enrichment. The shapes of the calcium phosphate grains suggest that they were mostly biogenic in origin. The grain size distributions of bulk sediments from the REY-enriched layers of cores PC04 (7.8–8.6 mbsf) and PC05 (2.6–3.6 mbsf) were bimodal, with peaks at fine (~4 μm) and coarse (~40–80 μm) sizes. Calcium phosphate and phillipsite were the major components of the coarse-grained portions of these REY-enriched layers. The bulk ∑REY content was mainly controlled by the amount of biogenic calcium phosphate, which is well known to concentrate REY. Thus, increased accumulation of biogenic calcium phosphate was responsible for the REY enrichment. The volume-based cumulative median diameters of calcium phosphate and phillipsite grains appeared to be proportional to the contents of both calcium phosphate and ∑REY. Increased phillipsite grain size suggests a low sedimentation rate, which may have allowed biogenic calcium phosphate to accumulate without dilution by low-∑REY components. In addition, increased grain sizes of calcium phosphate and phillipsite suggest that sorting by a bottom current allowed coarse-grained biogenic calcium phosphate to become concentrated in sediments by removing fine-grained particles, including low-∑REY components. Multiple factors should be considered to explain the overall features of the highly REY-enriched layers.

Keywords: REY-rich mud, biogenic calcium phosphate, phillipsite, pelagic sediment, grain size distribution

Introduction

Rare-earth elements and yttrium (REY) are essential elements in contemporary technology, and the demand for REY is expected to rise in the future (Alonso *et al*., 2012). For a stable supply capable of meeting an ever-rising demand for REY, diversification of sources and increased access to REY resources are critically needed. Recently, Kato *et al*. (2011) reported the existence of extensive new REY resources on the abyssal seafloor of many areas of the Pacific Ocean. They referred to pelagic sediment with total REY contents (∑REY) greater than 400 ppm as "REY-rich mud". By chemical analyses of sediment samples from two Deep Sea Drilling Project/Ocean Drilling Program (DSDP/ODP) cores (DSDP Hole 198A and ODP Hole 800A), Kato *et al*. (2012) identified REY-rich mud within the Japanese Exclusive Economic Zone around Minamitorishima Island (Minamitorishima

*Corresponding author (e-mail: ykato@sys.t.u-tokyo.ac.jp)

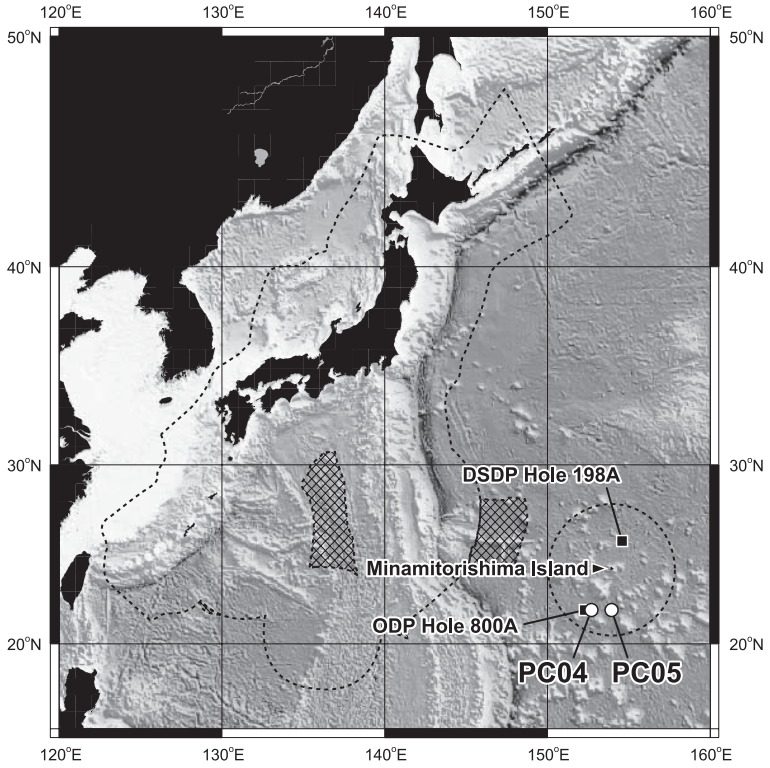

Fig. 1. Map showing locations of cores PC04 and PC05, modified from Fujinaga et al. (2016). Areas surrounded by dotted lines are the Japanese Exclusive Economic Zone and meshed sections are the areas of extended continental shelf.

EEZ) in the western North Pacific Ocean (Fig. 1).

After this discovery, the Japan Agency for Marine-Earth Science and Technology collected seven piston cores containing REY-rich mud from the seafloor approximately 250 km south of Minamitorishima Island during cruise KR13-02 of *R/V Kairei*. Several of these cores had much higher ∑REY contents than had been reported by Kato *et al*. (2011) (see Fujinaga *et al*., 2016). In particular, some portions of cores PC04 and PC05 (Fig. 1) exhibited very high ∑REY contents exceeding 4,000 ppm (Iijima *et al*., 2016). Iijima *et al*. (2016) have classified mud with ∑REY content of 2,000–5,000 ppm as "highly REY-rich mud" and mud with ∑REY content greater than 5,000 ppm as "extremely REY-rich mud". The mechanisms by which these mud layers acquired their high ∑REY contents are unresolved. Detailed characterization and quantification of the sedimentary constituents should provide important constraints on these mechanisms.

Components of REY-enriched pelagic sediments that are candidate hosts of the REY are Fe-Mn oxyhydroxides, Fe-Mn oxides, Ca phosphate, and possibly phillipsite. Fe-Mn oxyhydroxides are one of the well-known REY hosts (e.g., Jarvis, 1985; Barrett and Jarvis, 1988; German *et al*., 1990). German *et al*. (1990) reported that Fe-Mn oxyhydroxides in hydrothermal plumes scavenge REEs from seawater, enriching REEs in deep-sea sediments deposited in areas strongly influenced by hydrothermal activity. Fe-Mn oxides are also a known REY host (e.g., Bau *et al*., 1996, 2014; Hein *et al*., 2013), and biogenic Ca phosphate (BCP: fish teeth and bones, collectively referred to as fish debris) has long been reported to highly concentrate REY (e.g., Arrhenius *et al*., 1957; Bernat, 1975; Staudigel *et al*., 1985; Toyoda *et al*., 1990; Kashiwabara *et al*., 2014; Kon *et al*., 2014). In addition, Kato *et al*. (2011) reported that the zeolite mineral phillipsite may be an indicator mineral of REY enrichment in Pacific REY-rich muds. Phillipsite is a common authigenic mineral in pelagic sediments. Although phillipsite itself does not accommodate REY in its crystal lattice, REY-concentrating minerals incorporated in phillipsite aggregates have been suggested to contribute to REY enrichment (Dubinin, 2000).

In this study, we investigated the relationship between the abundance or occurrence of key components and REY enrichment in deep-sea sediment by analyzing the grain size distribution (GSD) of bulk sediments and of two components, Ca phosphate and phillipsite, that are characteristically observed in REY-rich mud (∑REY > 400 ppm) in the KR13-02 cores.

Table 1. Texture and mineral composition of the study samples estimated by microscopic observations

Sample number	Core-Section, Interval (cm)	Depth (mbsf)	∑REY (ppm)	Unit*	Texture (%)			Mineral composition (%)**						
					Clay	Silt	Sand	Clay-sized particles	Quartz	Feldspar	Phillipsite	Ca phosphate	Fe-Mn micronodules	Colored minerals
1	PC04-Sec. 2, 52–54	1.1	351	sc	80	20	0	80	15	2	<1	<1	<1	5
2	PC04-Sec. 3, 52–54	2.1	454	sc	90	10	0	90	4	—	7	<1	—	<1
3	PC04-Sec. 5, 52–54	4.0	472	zr	75	25	0	75	<1	—	25	2	—	—
4	PC04-Sec. 7, 52–54	6.0	571	zr	75	20	5	75	<1	—	25	<1	—	—
5	PC04-Sec. 9, 12–14	7.6	1200	zr	70	25	5	70	1	—	25	4	<1	—
6	PC04-Sec. 9, 52–54	8.0	3114	cr	65	25	10	65	<1	—	20	15	<1	—
7	PC04-Sec. 9, 82–84	8.3	4968	cr	60	20	20	60	<1	—	15	25	2	—
8	PC04-Sec. 10, 2–4	8.6	2104	lc	95	5	0	95	<1	—	<1	6	<1	—
9	PC04-Sec. 10, 42–44	9.0	1422	lc	90	10	0	90	<1	—	2	4	<1	—
10	PC04-Sec. 12, 42–44	11.0	1777	lc	90	10	0	90	<1	—	2	6	<1	—
1	PC05-Sec. 3, 22–24	1.5	659	uzr	70	20	10	70	<1	—	25	4	1	—
2	PC05-Sec. 3, 82–84	2.1	796	uzr	70	20	10	70	<1	—	30	1	1	—
3	PC05-Sec. 4, 62–64	2.9	3864	cr	70	15	15	70	<1	—	15	15	2	—
4	PC05-Sec. 4, 72–74	3.0	6799	cr	55	20	25	55	<1	<1	15	30	3	—
5	PC05-Sec. 4, 82–84	3.1	6596	cr	55	20	25	55	<1	—	15	25	4	—
6	PC05-Sec. 5, 22–24	3.5	3937	cr	70	15	15	70	<1	—	10	15	3	—
7	PC05-Sec. 5, 72–74	4.0	1057	lc	85	10	5	85	<1	—	7	7	<1	—
8	PC05-Sec. 6, 72–74	5.0	984	lc	90	10	0	90	<1	—	4	4	<1	—
9	PC05-Sec. 7, 82–84	6.1	725	lc	90	10	0	90	<1	—	4	2	<1	<1
10	PC05-Sec. 8, 82–84	7.1	2156	lc	85	15	0	85	<1	—	5	8	2	—
11	PC05-Sec. 9, 72–74	8.0	1120	lzr	75	20	5	75	<1	—	20	6	1	—
12	PC05-Sec. 10, 72–74	9.0	972	lzr	70	30	0	70	<1	—	30	3	<1	—

**Abbreviations: sc = surface clay; zr = zeolite-rich; cr = Ca phosphate-rich; lc = lower clay; uzr = upper zeolite-rich; lzr = lower zeolite-rich.*

***Values of more than 10% are rounded off to the nearest 5%.*

— = not detected.

Materials and Methods

Study samples

We selected two KR13-02 piston cores, PC04 and PC05, with layers of extremely or highly REY-rich mud (Iijima *et al*., 2016) for this study. Core PC04, 12.73 m long, was collected at 21°56.11′ N, 152°39.51′ E from 5,720 m water depth. Core PC05, 11.45 m long, was collected at 21°59.03′ N, 153°56.35′ E from 5,735 m water depth. The two core sites are ~130 km apart and approximately 250 km south of Minamitorishima Island (Fig. 1). The core sites are in a flat part of the seafloor surrounded by several seamounts belonging to the Marcus-Wake Seamount Chain. The cores consist mostly of macroscopically homogeneous brown to dark brown pelagic sediment without calcareous and siliceous biogenic components, referred to as pelagic brown clay (Iijima *et al*., 2016). Detailed lithologies and bulk chemical compositions (including REY) of these cores are reported elsewhere (Iijima *et al*., 2016; Fujinaga *et al*., 2016). A total of 22 sediment samples were collected from the cores with ~20 cm^3 scoops (10 samples from PC04 and 12 samples from PC05) for GSD analyses (Table 1). On the basis of lithologies reported by Iijima *et al*. (2016), this study classified the sediment columns of each core into units, as summarized below.

PC04: Core PC04 was classified into four units: in descending order, a surface clay unit (clay, 0.0–2.7 m below the seafloor (mbsf), ∑REY < ~500 ppm), a zeolite-rich unit (clay with zeolite or zeolitic clay, 2.7–7.9 mbsf, ∑REY = ~500–2,500 ppm), a Ca phosphate-rich unit (clay with phosphate and zeolite, 7.9–8.4 mbsf, ∑REY > ~2,500 ppm) and a lower clay unit (clay, 8.4 mbsf to the bottom, ∑REY = ~1,500–2,500 ppm). The Ca phosphate-rich unit basically corresponds to a layer of highly REY-rich mud (∑REY = 2,000–5,000 ppm). Samples were collected from each unit (Table 1).

PC05: Core PC05 was classified into five units: in descending order, a surface clay unit (clay, 0.0–0.5 mbsf, ∑REY < ~400 ppm), an upper zeolite-rich unit (clay with zeolite or zeolitic clay, 0.5–2.7 mbsf, ∑REY = ~400–2,500 ppm), a Ca phosphate-rich unit (clay with phosphate and zeolite, 2.7–3.5 mbsf, ∑REY > ~2,500 ppm), a lower clay unit (clay, 3.5–7.9 mbsf, ∑REY = ~700–3,000 ppm) and a lower zeolite-rich unit (clay with zeolite or zeolitic clay, 7.9 mbsf to the bottom, ∑REY = ~1,000–1,500 ppm). The Ca phosphate-rich unit of PC05 basically corresponds to a layer of highly to extremely REY-rich mud (∑REY > 2,000 ppm). The lower clay unit contains a thin (~30 cm in thickness) layer of clay with phosphate around 7.0 mbsf. Samples were collected from all units except the surface clay unit (Table 1).

Microscopic observations

To determine the detailed mineralogical characteristics of the samples, we estimated the proportions of each constituent (mineral compositions) and the proportions of clay-, silt- and sand-sized grains (textures) under a polarizing microscope following the protocols of the International Ocean Discovery Program (IODP) (Mazzullo and Graham, 1988). We categorized grains that were smaller than 4 μm as clay-sized particles (Table 1) because mineral identification of these grains is difficult under an optical microscope. We also observed the stereoscopic features of the Ca phosphate grains in the extremely REY-rich mud layer under a stereomicroscope and a scanning electron microscopy (SEM). The observed Ca phosphate grains were separated from the extremely REY-rich mud (PC05-Sec. 4, 72–74 cm) by using a 73-μm-mesh sieve (#200).

Grain size distribution analyses

In both cores, Ca phosphate and phillipsite were observed in the REY-rich mud under a microscope (Iijima *et al*., 2016; Fujinaga *et al*., 2016). In our GSD analysis, we focused on these two components and the bulk sediments. For the GSD analysis of bulk sediments, a ~1 g subsample was dispersed in ~10 mL of deionized Milli-Q water to make a slurry. The GSD of bulk sediments (GSD_{bulk}) was then determined by a Microtrac MT3000 laser diffraction spectroscopy in the University of Tokyo. We report the GSD of bulk sediments on a volume basis.

We also selected 13 samples (7 samples from PC04 and 6 samples from PC05, representing all units except for the surface clay unit of PC05) for GSD analyses of Ca phosphate and phillipsite. For each sample, the long (L) and short (S) axes of at least 400 grains of each mineral were manually measured on smear slides under a polarizing microscope. The long and short axes of Ca phosphate grains, which had irregular shapes, were measured so that each grain's flat face could be approximated as an ellipse. The long and short axes of phillipsite grains, which were prismatic, were measured along the principal crystal axes. The number of grains measured in each sample was statistically determined, assuming an infinite population with a normal distribution, to reasonably extract the grain characteristics of the sample. Because it is difficult to identify and measure clay-sized particles (<4 μm) under an optical microscope, we measured only silt- and sand-sized grains (>4 μm). We identified Ca phosphate and phillipsite on the basis of color, shape, refraction, interference colors and extinction angles.

The raw results, which were number-based distributions, were converted to volume-based distributions for quantitative comparison with the bulk GSDs. The volume of each phillipsite grain was estimated as $L \times S^2$, given the regular prismatic shape and square cross section of phillipsite grains. As shown later, the stereomicroscopic observation of the Ca phosphate grains

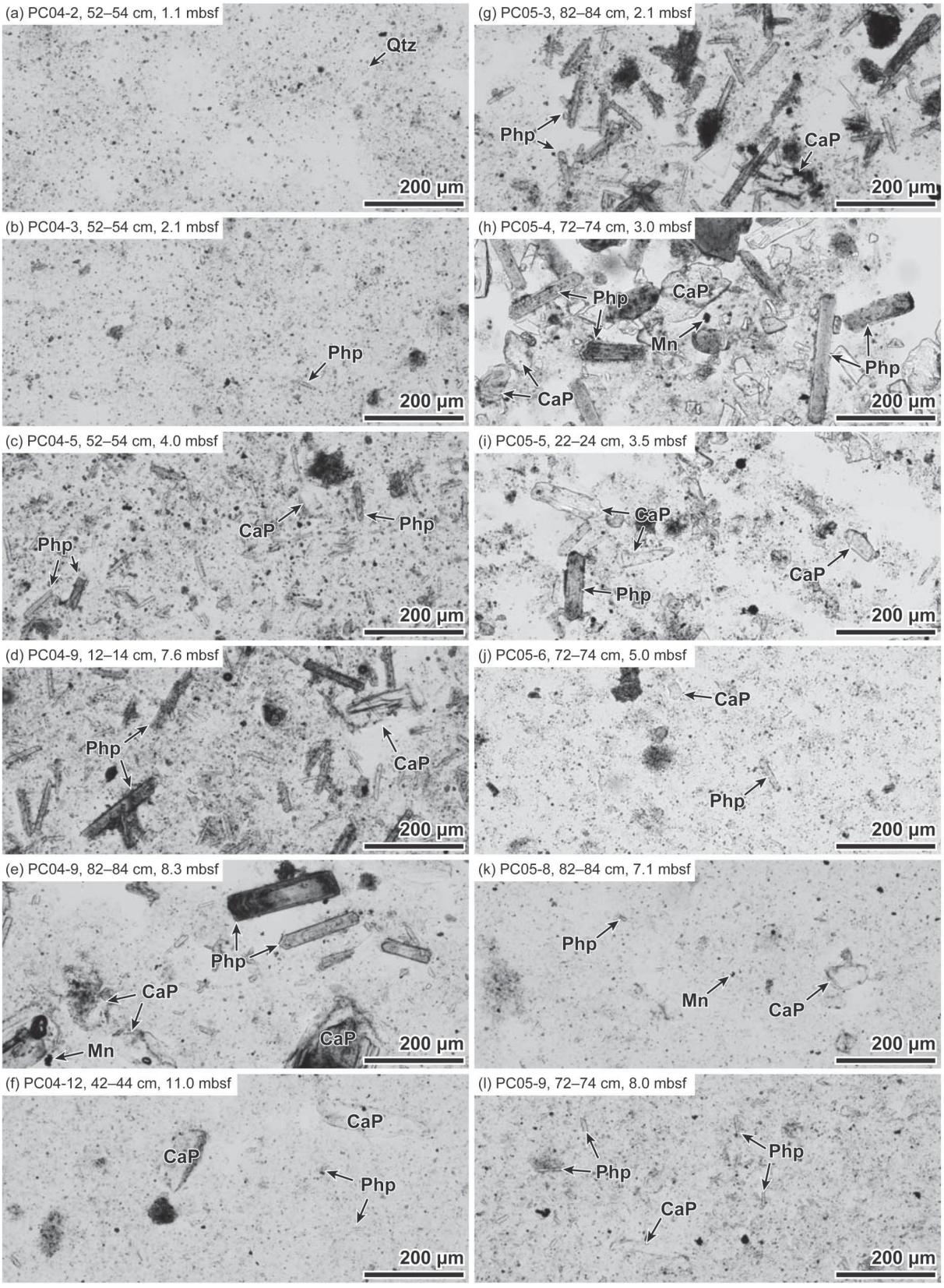

Fig. 2. Photomicrographs of representative samples from cores PC04 and PC05. CaP = Ca phosphate; Mn = Fe-Mn micronodules; Php = phillipsite; Qtz = quartz.

showed that a large fraction (~80%) of them was thin plates or thin columns with small variations in thickness. Therefore, we assumed a uniform thickness T and approximated the volume of the Ca phosphate grains as $1/4\pi \times L \times S \times T$. The actual value of T was not necessary because a uniform T was canceled out in the following calculation. The total volume fraction of the grains in diameter range i was calculated as V_i/V_{all}, where V_i is the total volume of the grains in range i and V_{all} is the total volume of all grains. These calculations yielded volume-based GSDs. We report the GSDs as distributions of the long axes for quantitative comparison with the bulk GSDs on the basis of following interpretation. The laser diffraction spectroscopy analysis measures a spherical locus in which randomly rotating grain draws in the introduced slurry. Thus, a grain diameter measured by the laser diffraction method is expected to be close to the long axis of the grain.

To characterize the GSDs of Ca phosphate and phillipsite, we calculated a volume-based cumulative median diameter (D50%) for each component, signifying the grain diameter at which the cumulative volume of the component reaches 50% of its total cumulative volume. This value is an appropriate measure of the average diameter when a GSD exhibits a skewed distribution.

Results

Mineralogical characteristics

The mineral compositions and textures of the samples, as estimated from the microscopic observations, are summarized in Table 1. Representative photomicrographs of the smear slides are shown in Fig. 2. The major characteristics of the two cores are described below.

PC04: The two samples from the surface clay unit of PC04 (Figs. 2a and 2b) consisted mostly of clay-sized particles, with very minor or minor amounts of quartz and very minor amounts of phillipsite, colored minerals and feldspar, mainly as grains smaller than medium silt (<16 μm). The three samples from the zeolite-rich unit (Figs. 2c and 2d) contained major amounts of phillipsite and very minor amounts of Ca phosphate and quartz. The phillipsite, Ca phosphate and quartz grains were 4 to ~100 μm, 4 to ~150 μm and ~5 μm in size, respectively. The two samples from the Ca phosphate-rich unit (Fig. 2e) contained moderate amounts of Ca phosphate, minor amounts of phillipsite and very minor amounts of Fe-Mn oxides (Fe-Mn micronodules). In this unit, the Ca phosphate and phillipsite grains were substantially larger than they were in other units (~4–400 μm and ~4–250 μm, respectively). The Fe-Mn micronodules in these samples were also larger (~20–500 μm) than in other samples with <1% Fe-Mn micronodules (several tens of micrometers). The three samples from the lower clay unit (Fig. 2f) consisted mostly of clay-sized particles with very minor amounts of Ca phosphate and phillipsite. The Ca phosphate grains ranged in size from 4 to ~200 μm, but the phillipsite grains were smaller and concentrated within the narrow size range (~4–30 μm).

PC05: The two samples from the upper zeolite-rich unit of PC05 (Fig. 2g) contained major amounts of phillipsite and very minor amounts of Ca phosphate and Fe-Mn micronodules. The Ca phosphate and phillipsite grains ranged in size from 4 to ~100 μm, and the Fe-Mn micronodules were around 20 μm. The four samples from the Ca phosphate-rich unit (Figs. 2h and 2i) contained moderate amounts of Ca phosphate, minor amounts of phillipsite and very minor amounts of Fe-Mn micronodules. Both the Ca phosphate (~4 to ~250 μm) and phillipsite (~4–200 μm) grains were occasionally quite large, and the Fe-Mn micronodule grains were larger (~20–200 μm) than in the other units. The four samples from the lower clay unit (Fig. 2j) consisted mostly of clay-sized particles with very minor amounts of Ca phosphate and phillipsite. One sample from this unit (PC05-Sec. 8, 82–84 cm) contained a very minor amount of relatively small (~20 μm) Fe-Mn micronodule grains. The Ca phosphate grains ranged in size from 4 to ~250 μm, and the phillipsite grains ranged in size from 4 to ~150 μm. The two samples from the lower zeolite-rich unit (Figs. 2k and 2l) contained moderate amounts of phillipsite, and very minor amounts of Ca phosphate and Fe-Mn micronodules. The phillipsite grains were small and concentrated within a narrow size range (~4–20 μm); the Ca phosphate grains ranged in size from 4 to ~150 μm and the Fe-Mn micronodule grains from ~10 to ~50 μm.

The stereomicroscopic observations of the Ca phosphate grains showed that they had various irregular shapes. To infer their origins, we categorized these shapes into five types: thin columns, thin plates, irregular grains with biological features, fossil fish teeth and opaque spheroidal agglomerations. We then visually estimated the fraction of each type by the method of Rothwell (1989). About 80% of the Ca phosphate grains had relatively simple shapes such as thin columns (Fig. 3a) or thin plates (Fig. 3b) with small variation in thickness, and were colorless and transparent. With their curved shapes and anisotropic or irregular structures, they were quite unlike grains of detrital crystalline apatite, which generally are euhedral hexagonal prisms or plates (e.g., Mange and Maurer, 1992). Instead, they were similar in shape to fossil fish debris reported by Trueman and Tuross (2002) and Gleason *et al*. (2009). In addition, they differed from apatite crystals in having obscure interference colors and in not displaying specific extinction angles. This is probably because BCP is an aggregation of nanocrystalline apatite (Trueman and Tuross, 2002). About 15% of the Ca phosphate grains had obviously biological features

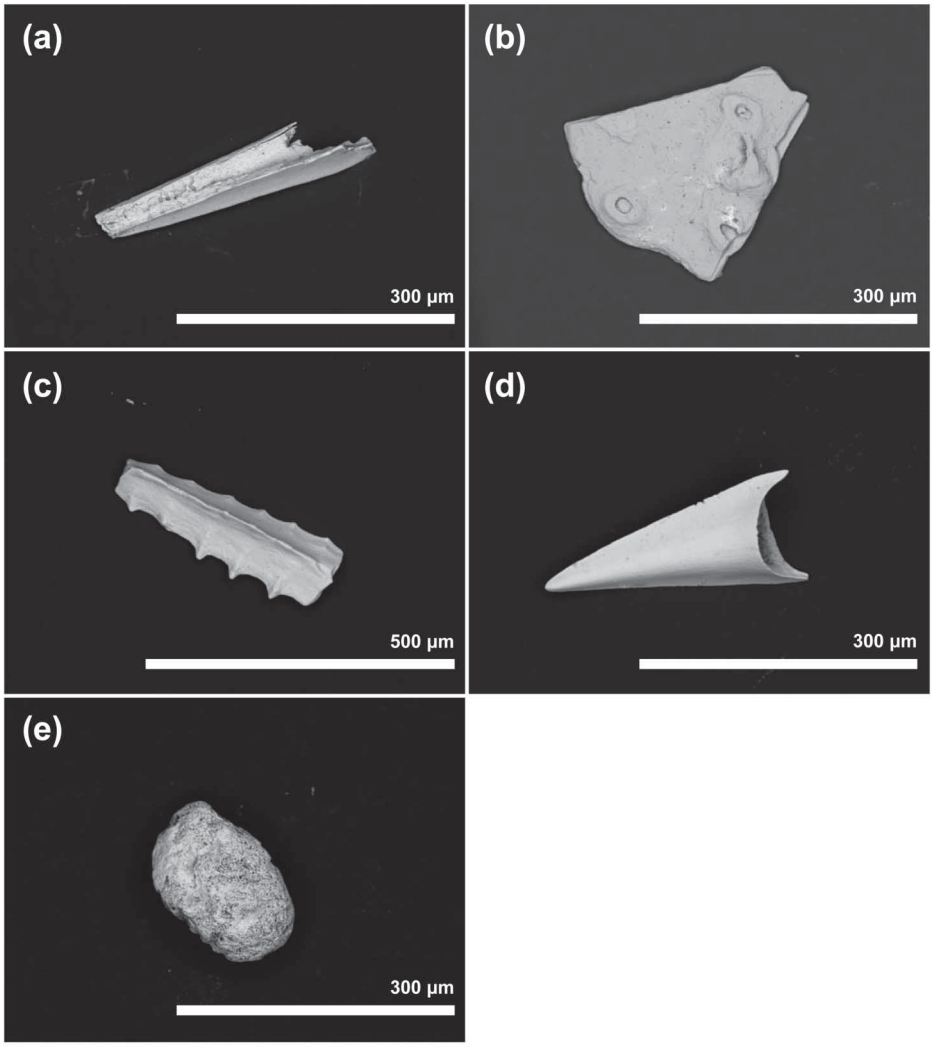

Fig. 3. SEM images of representative Ca phosphate grains from sample PC05-Sec. 4, 72–74 cm: (a) thin column (fossil fish debris), (b) thin plate (fossil fish debris), (c) irregular grain with biological feature, (d) fossil fish tooth and (e) opaque spheroidal agglomeration. The Ca phosphate grains were identified by energy-dispersive spectroscopy.

such as spurs and hollows (Fig. 3c) and had the same optical features as the thin columns and thin plates. A few (<1%) appeared to be fossil fish teeth (Fig. 3d). The rest (~5%) consisted of opaque spheroidal agglomerations (Fig. 3e) of obscure origin. We did not identify any crystalline apatite grains of likely detrital origin. Consequently, we considered almost all of the Ca phosphate grains in the layers of extremely REY-rich mud to be of biogenic origin. In the rest of this paper, Ca phosphate and BCP are treated as equivalent terms.

Grain size distributions

The grain size distributions of the bulk sediments (GSD_{bulk}) exhibited both unimodal and bimodal patterns (Figs. 4b and 5b). The samples with unimodal distributions had peaks at ~4 μm. Samples with bimodal distributions had finer and coarser peaks at ~4 μm (i.e., clay-sized particles) and ~40–80 μm (i.e., silt- and sand-sized grains), respectively. The D50% values for Ca phosphate and phillipsite ($D50\%_{CaP}$ and $D50\%_{php}$, respectively) are shown in Table 2. The principal characteristics of the GSDs in the two cores are as follows.

PC04: The GSD_{bulk} of the two samples from the surface clay unit of PC04 (samples 1 and 2) were unimodal (Fig. 4b). In the lower sample of the unit (sample 2), both $D50\%_{CaP}$ (18 μm) and $D50\%_{php}$ (23 μm) were larger than the ~4 μm peak in the GSD_{bulk} (Figs. 4b–d). In the three samples from the zeolite-rich unit (samples 3–5), the GSD_{bulk} were distinctly bimodal (Fig. 4b). The $D50\%_{CaP}$ of the top sample (sample 3) was 12 μm, between the two

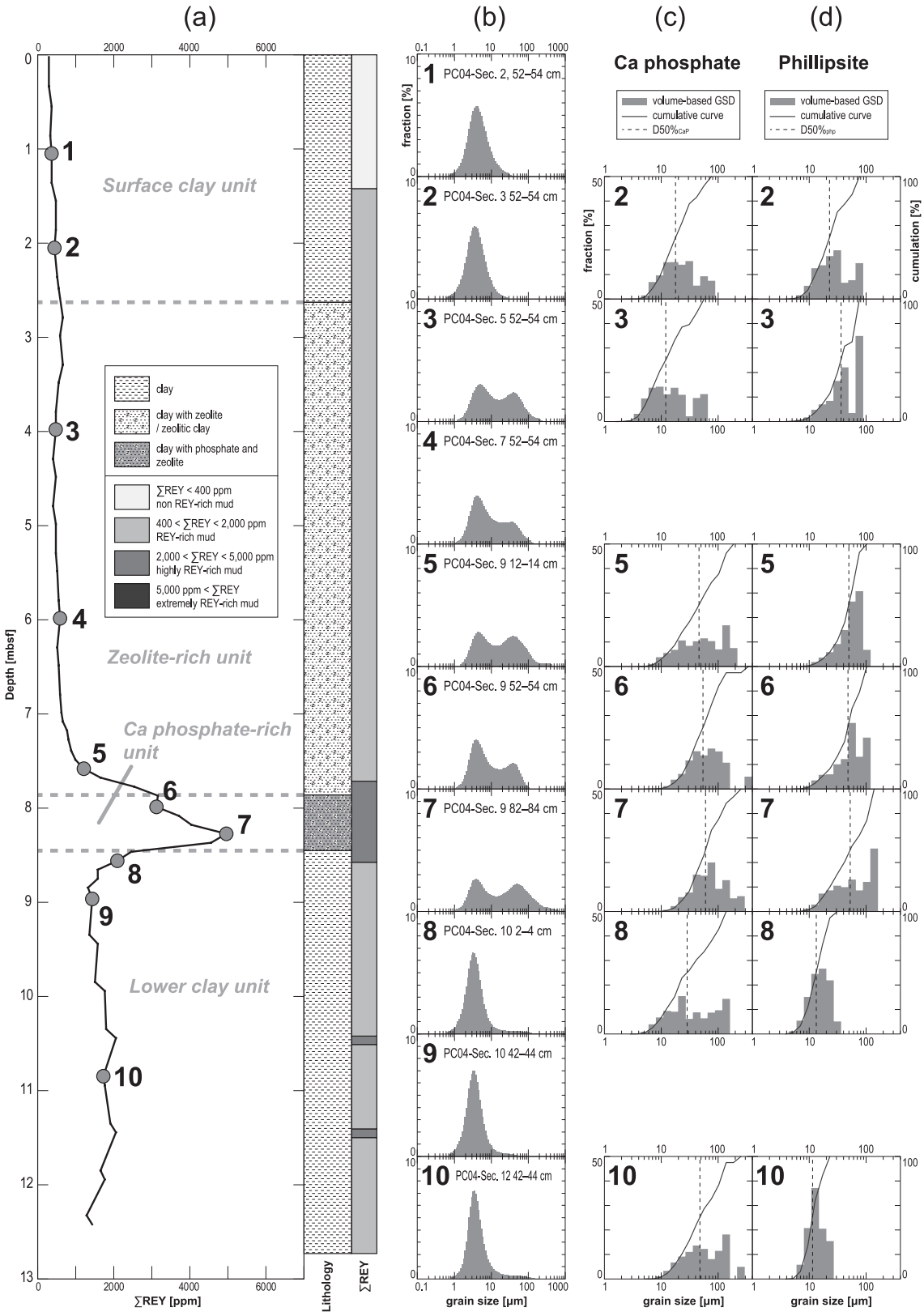

Fig. 4. Results of GSD analyses of core PC04. (a) Depth profiles of ∑REY contents with lithology, modified from Iijima et al. (2016). Gray circles indicate the points where bulk sediments were sampled for GSD analyses, with numbers corresponding to sample numbers in Tables 1 and 2. GSD analysis results from the samples marked in (a) for (b) bulk sediments, (c) Ca phosphate and (d) phillipsite. Grain size in (c) and (d) refers to the long axes.

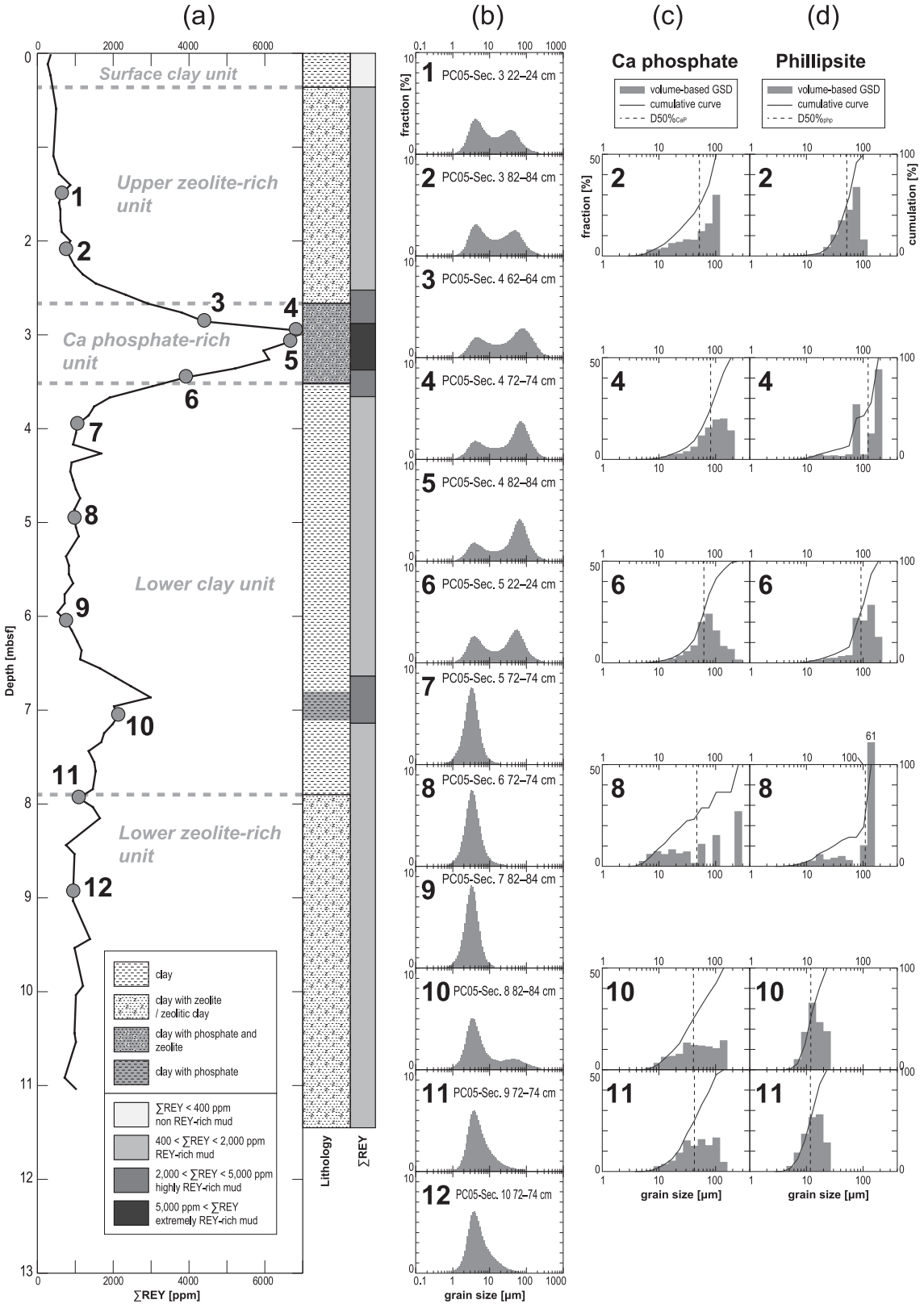

Fig. 5. Results of GSD analyses of core PC05. (a) Depth profiles of ∑REY contents with lithology, modified from Iijima et al. (2016), and GSD analysis results for (b) bulk sediments, (c) Ca phosphate and (d) phillipsite. Details are the same as in Fig. 4.

Table 2. Ca phosphate contents and D50% of Ca phosphate and phillipsite grains in analyzed samples.

Sample number*	Core-Section, Interval (cm)	Depth (mbsf)	∑REY (ppm)	Unit**	Mineral composition	GSD			
					Ca phosphate (BCP)	Ca phosphate		Phillipsite	
					(%)	*n****	D50% (μm)	*n****	D50% (μm)
2	PC04-Sec. 3, 52–54	2.1	454	sc	<1	415	18	425	23
3	PC04-Sec. 5, 52–54	4.0	472	zr	2	407	12	427	37
5	PC04-Sec. 9, 12–14	7.6	1200	zr	4	407	46	415	50
6	PC04-Sec. 9, 52–54	8.0	3114	cr	15	417	55	415	48
7	PC04-Sec. 9, 82–84	8.3	4968	cr	25	401	61	458	53
8	PC04-Sec. 10, 2–4	8.6	2104	lc	6	410	29	415	13
10	PC04-Sec. 12, 42–44	11.0	1777	lc	6	405	48	405	12
2	PC05-Sec. 3, 82–84	2.1	796	uzr	1	411	52	421	52
4	PC05-Sec. 4, 72–74	3.0	6799	cr	30	467	83	550	124
6	PC05-Sec. 5, 22–24	3.5	3937	cr	15	592	63	609	93
8	PC05-Sec. 6, 72–74	5.0	984	lc	4	410	47	420	110
10	PC05-Sec. 8, 82–84	7.1	2156	lc	8	448	41	437	12
11	PC05-Sec. 9, 72–74	8.0	1120	lzr	6	404	43	455	12

**Sample numbers correspond to those in Table 1.*
***Abbreviations: sc = surface clay; zr = zeolite-rich; cr = Ca phosphate-rich; lc = lower clay; uzr = upper zeolite-rich; lzr = lower zeolite-rich.*
****n = number of grains measured.*
Gray bands indicate samples showing the maximum ∑REY contents in each core.

peaks in the GSD_{bulk} (Figs. 4b and 4c), and that of the bottom sample (sample 5) was 46 μm, near the coarser peak in the GSD_{bulk} of ~40 μm (Figs. 4b and 4c). The $D50\%_{php}$ of these two samples were 37 and 50 μm, respectively, comparable to the coarser peaks in the GSD_{bulk} (Figs. 4b and 4c). In the two samples from the Ca phosphate-rich unit (samples 6 and 7), the GSD_{bulk} were bimodal, and both $D50\%_{CaP}$ (55 and 61 μm) and $D50\%_{php}$ (48 and 53 μm) were comparable to the coarser GSD_{bulk} peaks of ~40–50 μm (Figs. 4b–d). In the three samples from the lower clay unit (samples 8–10), the GSD_{bulk} were unimodal (Fig. 4b). The $D50\%_{CaP}$ of the top and bottom samples (samples 8 and 10) were 29 and 48 μm, respectively, much larger than the ~4 μm peaks in the GSD_{bulk} (Figs. 4b and 4c). In contrast, the $D50\%_{php}$ of these samples (13 and 12 μm, respectively) were only slightly larger than the GSD_{bulk} peaks (Figs. 4b and 4d). In addition, the GSD for phillipsite (GSD_{php}) of these two samples were narrower than those of the samples from the other units (Fig. 4d).

PC05: The GSD_{bulk} of the two samples from the upper zeolite-rich unit (samples 1 and 2) were distinctly bimodal (Fig. 5b). In the lower sample (sample 2), $D50\%_{CaP}$ (52 μm) and $D50\%_{php}$ (52 μm) were near the coarser peak in the GSD_{bulk} of ~50 μm (Figs. 5b–d). In the four samples from the Ca phosphate-rich unit (samples 3–6), the GSD_{bulk} were bimodal (Fig. 5b). In two samples from this unit (samples 4 and 6), $D50\%_{CaP}$ (83 and 63 μm, respectively) were close to the coarser peaks in the GSD_{bulk} (Figs. 5b and 5c), whereas $D50\%_{php}$ (124 and 93 μm, respectively) were larger (Figs. 5b and 5d). The GSD_{bulk} of the upper three samples from the lower clay unit (samples 7–9) were unimodal (Fig. 5b). In one of these samples (sample 8), both $D50\%_{CaP}$ (47 μm) and $D50\%_{php}$ (110 μm) were much larger than the GSD_{bulk} peak (Figs. 5b–d). In contrast, the GSD_{bulk} of the sample from the bottom of the unit (sample 10) had a bimodal pattern with a relatively small coarser peak (Fig. 5b). In this sample, $D50\%_{CaP}$ (41 μm) was close to the coarser peak in the GSD_{bulk} of ~40–50 μm, whereas $D50\%_{php}$ (12 μm) was between the two peaks in the GSD_{bulk} (Figs. 5b–d). In addition, the GSD_{php} in this sample was narrower than in the samples above it (Fig. 5d). In the two samples from the lower zeolite-rich unit (samples 11 and 12), the GSD_{bulk} were unimodal (Fig. 5b). In the upper sample of this unit (sample 11), $D50\%_{CaP}$ (43 μm) was much larger, and $D50\%_{php}$ (12 μm) was slightly larger, than the GSD_{bulk} peak of ~4 μm (Figs. 5b–d), and the GSD_{php} was also narrow, similar to that in sample 10 from the lower clay unit (Fig. 5d).

DISCUSSION

Components forming the peaks in the GSD_{bulk}

In the upper three units of PC04 and PC05, both $D50\%_{CaP}$ and $D50\%_{php}$ were larger than both the peaks in unimodal GSD_{bulk} and the finer peaks in bimodal GSD_{bulk}, and comparable to the coarser peaks in bimodal GSD_{bulk}. Because BCP and phillipsite accounted for large portions (>25%) of the sediments with bimodal GSD_{bulk} (Table 1), we inferred that the coarser peaks represent BCP and phillipsite, whereas the finer peaks represent the domi-

nant clay-sized particles in the cores. In addition, the coarser peaks grew higher than the finer peaks in the GSD_{bulk} as the total content of BCP and phillipsite increased (Figs. 4 and 5, Table 1). Moreover, BCP exceeded phillipsite in the layer of extremely/highly REY-rich mud (Table 1). These findings suggest that coarse-grained components, especially BCP, were responsible for the extremely/highly REY-rich mud.

In the lower clay units of both cores, the GSD_{bulk} was unimodal (except for sample 10 of PC05). The single peaks in the GSD_{bulk} at ~4 μm reflected the great predominance of clay-sized particles (Table 1). Although $D50\%_{CaP}$ and $D50\%_{php}$ were both greater than ~4 μm, BCP and phillipsite were too scarce to form coarser peaks in the GSD_{bulk} except in sample 10 of PC05, in which a relatively large proportion of BCP (~8%) accounted for the small coarser peak in the GSD_{bulk} (Fig. 5b). In the lower zeolite-rich unit of PC05 (samples 11 and 12), the GSD_{bulk} were unimodal even as phillipsite constituted ~20–30% of the samples. Because $D50\%_{php}$ was unusually small in this unit, as in the lower clay unit of PC04 and the bottom sample of the lower clay unit of PC05, the phillipsite grains probably had long-tailed distributions, extending toward large grain sizes, in the GSD_{bulk} (Fig. 5b).

Comparison of lithology, ∑REY contents and GSDs in cores PC04 and PC05

The lithologies, ∑REY contents and GSDs of the upper three units of PC04 were similar to those of the corresponding units in PC05. In both cores, the surface clay units had clay lithologies and their ∑REY contents were low (<~500 ppm) (Figs. 4a and 5a). The relatively high quartz content in the surface clay unit of PC04 (Table 1) probably reflects that an eolian component sedimentation in the western North Pacific Ocean has significantly increased since the Neogene (e.g., Janecek, 1985). The zeolite-rich unit of PC04 and the upper zeolite-rich unit of PC05 both contained major amounts of phillipsite (Table 1), had moderate ∑REY contents (~500–2,500 ppm) and had bimodal GSD_{bulk} patterns (Figs. 4a, 4b, 5a and 5b). The Ca phosphate-rich units of the two cores contained major amounts of both BCP and phillipsite (Table 1), had very high ∑REY contents (>~2,500 ppm) and had bimodal GSD_{bulk} patterns (Figs. 4a, 4b, 5a and 5b). Although the upper three units differed in thickness between PC04 and PC05, their similarities suggest that these units were formed by similar geological processes.

In contrast, the sediment characteristics of the underlying units of PC04 and PC05 differed. PC04 contained only clay sediments (the lower clay unit), whereas in PC05 clay sediments graded downward into zeolite-rich clay (lower clay unit to lower zeolite-rich unit) (Figs. 4a and 5a). PC05 included a layer with a bimodal GSD_{bulk} at 7.1 mbsf (sample 10), whereas all of the GSD_{bulk} in PC04 were unimodal (Figs. 4b and 5b). The lower clay units of PC04 and PC05 were similar in their clay-rich lithologies. However, PC04 differed from PC05 in that its GSD_{php} were narrow and its $D50\%_{php}$ were small, more closely resembling the lower zeolite-rich unit of PC05. It may be that PC04 lacked a layer corresponding to the lower clay unit of PC05. In any case, these differences between PC04 and PC05 imply that local geological conditions differed between PC04 and PC05 when the units below the Ca phosphate-rich units were being deposited.

Implications for the formation of the extremely/highly REY-rich mud

The layers of extremely/highly REY-rich mud (i.e., the Ca phosphate-rich unit of PC04 and the Ca phosphate rich-unit and the bottom sample of the lower clay unit of PC05) contained larger amounts of BCP (~15–30%) than the other layers (less than 8%) (Table 1). In addition, the amounts of BCP appeared to be proportional to the ∑REY contents in all units (Table 1). BCP has long been reported to concentrate REY in deep-sea sediments (e.g., Arrhenius *et al*., 1957; Staudigel *et al*., 1985; Toyoda *et al*., 1990; Kashiwabara *et al*., 2014; Kon *et al*., 2014). Given an average ∑REY content in BCP of ~21,000 ppm (Kon *et al*., 2014), sediments with 7,000 ppm REY then need to contain ~33% BCP. This value is comparable to the BCP content in the extremely REY-rich mud layer of PC05 (~30%). In addition, ∑REY and P_2O_5 contents of all the samples from the Minamitorishima EEZ are plotted along the mixing line between detrital component and BCP (Fujinaga *et al*., 2016). Therefore, we attribute the presence of extremely/highly REY-rich mud to the accumulation of BCP in a thin sedimentary horizon. This may simply reflect an increased supply of BCP to the seafloor. Although, the accumulation of BCP is mainly responsible for the extreme/high REY-enrichment, the grain sizes of BCP ($D50\%_{CaP}$), as well as phillipsite ($D50\%_{php}$), appeared to be proportional to both BCP and ∑REY contents, reaching their maximum values in the layers of extremely/highly REY-rich mud (Table 2). These suggest that the factor or factors promoting increased grain sizes of BCP and phillipsite account for the anomalous increase in the amount of BCP, and thus for the extraordinary REY-enrichment of these layers.

The increased grain size of phillipsite cannot be directly related to increased REY concentrations, because phillipsite crystals themselves do not incorporate REY (Dubinin, 2000; Kon *et al*., 2014). Instead, it appears that the larger grain size of phillipsite reflects factors that also control the accumulation of BCP (which contains REY) in pelagic sediment. It has long been known that phillipsite crystals grow when sedimentation is relatively slow, as is typical in deep-sea basins covered by pelagic clay (Bernat *et al*., 1970; Stonecipher, 1976). Czyscinski

(1973) reported that the growth of phillipsite crystals was the most rapid in the top 10 cm interval of a pelagic clay core from the Indian Ocean. This suggests that the growth of large phillipsite grains may reflect a low sedimentation rate resulting in long-term exposure of the crystals on the seafloor. In our analyses, $D50\%_{php}$ and BCP contents increased simultaneously (Table 2), indicating that large phillipsite crystals coincide with enhanced accumulation of BCP. We attribute this association to a low sedimentation rate due to a depressed accumulation of components with low ∑REY contents (e.g., detrital component, biogenic carbonate or silica). A low sedimentation rate thus may simultaneously allow BCP to accumulate without dilution by low-∑REY components, and allow phillipsite crystals to grow larger. Moreover, a low sedimentation rate would also allow BCP to concentrate REY sufficiently. Previous work has indicated that REY contents of BCP are several orders of magnitude lower in living organisms than in pelagic clay (Elderfield and Pagett, 1986). Yasukawa *et al*. (2015) noted that BCP can acquire REY from seawater during prolonged exposure to the seawater near the sediment surface when sedimentation rates are sufficiently low. Slow sedimentation thus appears to be an important requisite to form REY-rich mud.

Another factor that may affect the particle size distribution in sediment is strong bottom currents, which tend to remove finer (mainly silt-sized) particles and leave coarser particles (e.g., McCave *et al*., 1995). Such sorting would concentrate coarser grains of BCP and phillipsite by removing finer grains. Because BCP is an originally coarse-grained material, the result would be an increase in the BCP fraction of the sediment. The conjunction of high $D50\%_{CaP}$, $D50\%_{php}$, and BCP and ∑REY contents (Table 2) would imply that sorting also contributes to the formation of extremely/highly REY-rich mud.

Our results, then, suggest that the formation of extremely/highly REY-rich mud resulted from a combination of an increased supply of BCP to the seafloor, a low sedimentation rate, and sorting of sediment particles by strong bottom currents. The extraordinary REY-enrichment in a thin sedimentary horizon implies that these factors were associated with a relatively brief geological event. The actual causes and relative contributions of these factors to REY enrichment remain uncertain. Detailed paleoceanographic and chronological information may provide useful insights into both the mechanisms forming extremely/highly REY-rich mud and the potential distribution of a novel REY resource of economic interest.

Conclusions

We conducted microscopic observations and GSD analyses of KR13-02 cores PC04 and PC05, which contain layers of extremely/highly REY-rich mud. The upper three units in PC04 are similar in lithology, ∑REY contents and GSDs to the corresponding units in PC05. Microscopic observations of sediment samples from the cores revealed that the layers of extremely/highly REY-rich mud contained substantial amounts of biogenic Ca phosphate that probably contributed to the REY enrichment of the mud. These layers also contained large phillipsite grains, implying a low sedimentation rate. The bulk GSDs of the extremely/highly REY-rich mud were distinctly bimodal, with a finer peak representing clay-sized particles and a coarser peak representing abundant grains of Ca phosphate and phillipsite. In both cores, the Ca phosphate contents were proportional to the ∑REY contents, suggesting that biogenic Ca phosphate was responsible for the extreme degree of REY enrichment. The volume-based cumulative median diameters (D50%) of Ca phosphate and phillipsite grains also were proportional to the Ca phosphate and ∑REY contents. The increased grain size of phillipsite, indicative of a low sedimentation rate, suggests that slow sedimentation allowed Ca phosphate to accumulate without dilution by other components. The increased grain sizes of both Ca phosphate and phillipsite are also consistent with grain-size sorting by bottom currents that helped concentrate coarse-grained biogenic Ca phosphate. We suggest that some combination of these factors contributed to the REY enrichment in the extremely/highly REY-rich mud.

Acknowledgments—This study used samples provided by the Japan Agency for Marine-Earth Science and Technology. We thank Y. Ichiyama and staff members at the Kochi Core Center for their assistance with the sampling. We thank Prof. T. Fujita, Assoc. Prof. G. Dodbiba and S. Masao for the bulk grain-size analysis. This research was financially supported by the Japan Society for the Promotion of Science (JSPS) through Grants-in-Aid for JSPS Fellows No. 14J10351 to J.O., for Scientific Research (S) No. 22226015 and No. 15H05771 to Y.K., and for Scientific Research (B) No. 25289334 to K.N.

References

Alonso, E., Sherman, A. M., Wallington, T. J., Everson, M. P., Field, F. R., Roth, R. and Kirchain, R. E. (2012) Evaluating rare earth element availability: A case with revolutionary demand from clean technologies. *Environ. Sci. Technol.* **46**, 3406–3414.

Arrhenius, G., Bramlette, M. N. and Picciotto, E. (1957) Localization of radioactive and stable heavy nuclides in ocean sediments. *Nature* **180**, 85–86.

Barrett, T. J. and Jarvis, I. (1988) Rare-earth element geochemistry of metalliferous sediments from DSDP Leg 92: The East Pacific Rise transect. *Chem. Geol.* 67, 243–259.

Bau, M., Koschinsky, A., Dulski, P. and Hein, J. R. (1996) Comparison of the partitioning behaviours of yttrium, rare earth

elements, and titanium between hydrogenetic marine ferromanganese crusts and seawater. *Geochim. Cosmochim. Acta* **60**, 1709–1725.

Bau, M., Schmidt, K., Koschinsky, A., Hein, J., Kuhn, T. and Usui, A. (2014) Discriminating between different genetic types of marine ferro-manganese crusts and nodules based on rare earth elements and yttrium. *Chem. Geol*. **381**, 1–9.

Bernat, M. (1975) Les isotopes de l'uranium et du thorium et les terres rares dans l'environnement marin. *Cah. ORSTOM. Sér. Géol*. **7**, 65–83.

Bernat, M., Bieri, R. H., Koide, M., Griffin, J. J. and Goldberg, E. O. (1970) Uranium, thorium, potassium and argon in marine phillipsites. *Geochim. Cosmochim. Acta* **34**, 1053–1071.

Czyscinski, K. (1973) Authigenic phillipsite formation rates in the central Indian Ocean and the Equatorial Pacific Ocean. *Deep-Sea Res*. **20**, 555–559.

Dubinin, A. V. (2000) Geochemistry of rare earth element in oceanic phillipsites. *Lithol. Miner. Resour*. **35**, 101–108.

Elderfield, H. and Pagett, R. (1986) Rare earth elements in ichthyoliths: Variations with redox conditions and depositional environment. *Sci. Total Environ*. **49**, 175–197.

Fujinaga, K., Yasukawa, K., Nakamura, K., Machida, S., Takaya, Y., Ohta, J., Araki, S., Liu, H., Usami, R., Maki, R., Haraguchi, S., Nishio, Y., Usui, Y., Nozaki, T., Yamazaki, T., Ichiyama, Y., Ijiri, A., Inagaki, F., Machiyama, H., Iijima, K., Suzuki, K., Kato, Y. and KR13-02, MR13-E02 Leg 2 and KR14-02 Cruise Members (2016) Geochemistry of REY-rich mud in the Japanese Exclusive Economic Zone around Minamitorishima Island. *Geochem. J*. **50**, this issue, 575–590.

German, C. R., Klinkhammer, G. P., Edmond, J. M., Mitra, A. and Elderfield, H. (1990) Hydrothermal scavenging of rare-earth elements in the ocean. *Nature* **345**, 516–518.

Gleason, J. D., Thomas, D. J., Moore, T. C., Jr., Blum, J. D., Owen, R. M. and Haley, B. A. (2009) Early to middle Eocene history of the Arctic Ocean from Nd-Sr isotopes in fossil fish debris, Lomonosov Ridge. *Paleoceanography* **24**, PA2215, doi:10.1029/2008PA001685.

Hein, J. R., Mizell, K., Koschinsky, A. and Conrad, T. A. (2013) Deep-ocean mineral deposits as a source of critical metals for high- and green-technology applications: Comparison with land-based resources. *Ore Geol. Rev*. **51**, 1–14.

Iijima, K., Yasukawa, K., Fujinaga, K., Nakamura, K., Machida, S., Takaya, Y., Ohta, J., Haraguchi, S., Nishio, Y., Usui, Y., Nozaki, T., Yamazaki, T., Ichiyama, Y., Ijiri, A., Inagaki, F., Machiyama, H., Suzuki, K., Kato, Y. and KR13-02 Cruise Members (2016) Discovery of extremely REY-rich mud in the western North Pacific Ocean. *Geochem. J*. **50**, this issue, 557–573.

Janecek, T. R. (1985) Eolian sedimentation in the Northwest Pacific Ocean: A preliminary examination of the data from Deep Sea Drilling Project Sites 576 and 578. *DSDP Init. Repts*. **86** (Heath, G. R., Burckle, L. H., D'Agostino, A. E., Bleil, U., Horai, K., Jacobi, R. D., Janecek, T. R., Koizumi, I., Krissek, L. A., Monechi, S., Lenôtre, N., Morley, J. J., Schultheiss, P. and Wright, A. A., eds.), 589–603, U.S. Government Printing Office, Washington, D.C.

Jarvis, I. (1985) Geochemistry and origin of Eocene-Oligocene metalliferous sediments from the central equatorial Pacific: Deep Sea Drilling Project sites 573 and 574. *DSDP Init. Repts*. **85** (Mayer, L., Theyer, F., Barron, J. A., Dunn, D. A., Handyside, T., Hills, S., Jarvis, I., Nigrini, C. A., Pisias, N. C., Pujos, A., Saito, T., Stout, P., Thomas, E., Weinreich, N. and Wilkens, R. H., eds.), 781–804, U.S. Government Printing Office, Washington, D.C.

Kashiwabara, T., Toda, R., Kato, Y., Fujinaga, K., Takahashi, Y. and Honma, T. (2014) Determination of host phase of lanthanum in deep-sea REY-rich mud by XAFS and μ-XRF using high-energy synchrotron radiation. *Chem. Lett*. **43**, 199–200.

Kato, Y., Fujinaga, K., Nakamura, K., Takaya, Y., Kitamura, K., Ohta, J., Toda, R., Nakashima, T. and Iwamori, H. (2011) Deep-sea mud in the Pacific Ocean as a potential resource for rare-earth elements. *Nat. Geosci*. **4**, 535–539.

Kato, Y., Fujinaga, K., Takaya, Y., Nakamura, K. and Iwamori, H. (2012) Is deep-sea mud a promising resource for rare-earth elements? *Abstracts with programs, the Society of Resource Geology* **62**, 37 (abstr.).

Kon, Y., Hoshino, M., Sanematsu, K., Morita, S., Tsunematsu, M., Okamoto, N., Yano, N., Tanaka, M. and Takagi, T. (2014) Geochemical characteristics of apatite in heavy REE-rich deep-sea mud from Minami-Torishima Area, southeastern Japan. *Resour. Geol*. **64**, 47–57.

Mange, M. A. and Maurer, H. (1992) *Heavy Minerals in Colour*. Springer, 147 pp.

Mazzullo, J. and Graham, A. G. (1988) *Handbook for Shipboard Sedimentologists*. *ODP Technical Note 8*. Ocean Drilling Project, 67 pp.

McCave, I. N., Manighetti, B. and Robinson, S. G. (1995) Sortable silt and fine sediment size/composition slicing: Parameters for palaeocurrent speed and palaeoceanography. *Paleoceanography* **10**, 593–610.

Rothwell, R. G. (1989) *Minerals and Mineraloids in Marine Sediments: An Optical Identification Guide*. Elsevier, 296 pp.

Staudigel, H., Doyle, P. and Zindler, A. (1985) Sr and Nd isotope systematics in fish teeth. *Earth Planet. Sci. Lett*. **76**, 45–56.

Stonecipher, S. A. (1976) Origin, distribution and diagenesis of phillipsite and clinoptilolite in deep-sea sediments. *Chem. Geol*. **17**, 307–318.

Toyoda, K., Nakamura, Y. and Masuda, A. (1990) Rare earth elements of Pacific pelagic sediments. *Geochim. Cosmochim. Acta* **54**, 1093–1103.

Trueman, C. N. and Tuross, N. (2002) Trace elements in recent and fossil bone apatite. *Rev. Mineral. Geochem*. **48** (Kohn, M. L., Rakovan, J. and Hughes, J. M., eds.), 489–522, Mineral. Soc. Am.

Yasukawa, K., Nakamura, K., Fujinaga, K., Machida, S., Ohta, J., Takaya, Y. and Kato, Y. (2015) Rare-earth, major, and trace element geochemistry of deep-sea sediments in the Indian Ocean: Implications for the potential distribution of REY-rich mud in the Indian Ocean. *Geochem. J*. **49**, 621–635.